The First National Conference on Mechanical Engineering
MOSTEFA BENBOULAID BATNA 2 UNIVERSITY
FACULTY OF TECHNOLOGY - MECHANICAL ENGINEERING DEPARTMENT
Département de
GENIE MECANIQUE
NCME'23

Research Paper

Contribution to analysis and friction exploitation as part of the improvement in terms of industrial robot repeatability

Rezala Aicha

Department of Mechanical and Production Engineering, Mechanical and Process Engineering Faculty, University of Science and Technology Houari Boumediene (USTHB), B.P. 32, El-Alia, 16111, Bab-Ezzouar, Algiers, Algeria

ARTICLE INFO

Article history:

Received 01 February 2023

Accepted 05 May 2023

Keywords:

Repeatability; asperity; friction; industrial robot

ABSTRACT

The imperfections at the origin of the lack of repeatability are of random nature, caused by the adjustments of the servo-control and especially by non-geometric phenomena such as the play and friction existing at the joints level. The occurring friction constitutes one of the main causes of performance loss. The friction modeling isn't an easy task, and therefore, its correction in advance remains difficult. The adopted method consisted of employing mechanical approaches in order to theoretically identify the contribution of friction on the pose repeatability. The tribological experimental study was carried out on the alternative tribometer and is based on the steel grade 42CD4 with a steel pin 100C6 used on the robot joints. Due to the variability of the friction values coefficient, the main asperities on isotropic surfaces were analyzed by considering their characteristics, namely the top altitude of each asperity, the distance between two consecutive views, and its radius. Each of these geometric characteristics is described using statistical analysis with probability density functions such as Gaussian laws. Finally, these developments resulted in a model that was applied by using measurements of three different types of microgeometry, ranging from quasi-periodic to quasi-random. The obtained results are interesting because they served to improve the analysis of repeatability by taking into account the friction phenomenon.

1 Introduction

The performance characteristics of industrial robots, as well as the test methods, are provided by ISO 9283 [1] and ANSI / RIA (1990). The first considered standard gives the definitions of the pose and orientation repeatability. This is always useful when the different causes of position and orientation errors of the industrial robot terminal organ are sought. The pose repeatability characterizes the poses dispersion reached by the robot to attain the same point several times. It is always tough for a robot to execute a same positioning in the case of a repeated trajectory hence the existence of errors to be rectified. The situation is improved by adding corrections resulting from the geometric model calibration. Adding to this, other purely random natural fluctuations cause a particular dispersion in the positioning of the industrial robot. Thereby, friction, clearances, connections wear, electrical noise, encoder resolution, hysteresis, servo-control settings, and other stochastic errors represent the deviations in poses causing the repeatability defect. In order to have the factors which act on the industrial robot's repeatability, statistical studies are carried out by Ramsli [2] and Edan [3]. Riemer [4] is particularly interested in the influence of location in the workspace. Offodile and Ugwu focus on the influence of load and speed [5]. However, work on the subject is still unfinished. Consequently, the interest of the studies carried out by GREAH on industrial robots to measure the impact of several influencing factors on the pose repeatability.

* *Corresponding author.* E-mail address: aicha.rezala@usthb.edu.dz

Ten years of research in this field at the GREAH laboratory [6,7] have been demonstrated the predominant robots factor with rotoid joints lies in the target location in the workspace. Typically, industrial robots are exposed to the frictional force that manifests at each point where two surfaces in relative motion come into contact. Numerous studies have been carried out to better analyze friction at the level of joints, reducers, transmissions, and scientists have concluded that proper friction management is a constant challenge in the design of an industrial robot [8]. One of the first presentations to use this kind of model is found in Coulomb's work (1782). To explain the law of friction, he assumed that the asperities possessed a spherical shape, all of which had the same radius and the same summit altitude. However, uncompensated friction causes positioning errors, delays, and limit cycles. Hence, the interest in seeking precise modeling of friction behavior requires a model of friction forces based on the joint's actual behavior. Our method is based on the theoretical identification of the friction contribution that shows the pose repeatability, and it also consists of the statistical study of the friction coefficient values. In this case, our analysis concerns microgeometric defects and, in particular, those are forming the main asperities. Thus, like the vast majority of authors [9-12], it's preferable to develop a model based on asperities using a spherical shape. However, in all cases, it is useful to establish a theoretical link between the functional properties of the surface and its microgeometry. According to this approach, before modelling the behavior of the surface, it is necessary to analyze the morphology of the surface and try to describe it with the most relevant details. For this, the use of these universal standardized parameters and develop a statistical description of asperity shapes and positions available on an extensive range of microgeometry from periodic to random profiles is favored.

2 Comparison between numerical and real application

The proposed robot is a Cartesian robot with prismatic articulation. The latter is a mechanical element which allows two consecutive segment bodies to be linked while smoothing a degree of freedom (1ddl). The output function is a translation along the x axis obtained by a series of transformations of movements. This transformation is assured by mechanisms: engine, screw/nut, gear, etc… The translation arm is assimilated to a segment, which slides on a slide fixed to the built, as shown in Figure.1. Position repeatability is determined at the end of the segment. Figure 2 shows the kinematic diagram of the robot.

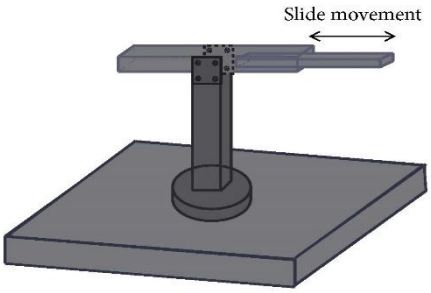

Fig. 1 - Structure of a typical industrial robot.

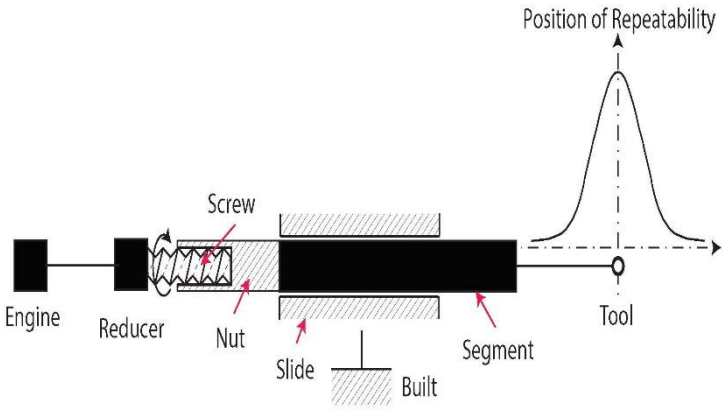

Fig. 2 - Kinematic diagram of the proposed robot [13].

The robot studied can be schematized by the junction of two bodies of complementary functions. The first body consists of the transmission mechanism: engine-slide. A spring of rigidity k can idealize this part. The second body corresponds to the segment-slide part. An alternative translation tribometer can symbolize the latter. Therefore, the sources of errors requesting the repeatability dispersion will be listed in two classes:

- The first class of error brings together all mechanical and geometric errors (alignment, vibration, force, adjustment) noted ε_t.
- The second error class contains the friction errors (friction coefficient, mechanical games, energy loss) noted ε_D.

Therefore, the robot can be schematized by Figure 3, where it is detailed in the tribological part Segment-Slide of the robot proposed by a contact Pin-Plate from the alternative tribometer to idealize the movement and simplify the positioning of the effector (output element). In addition, it is assumed that the mechanical contribution (elasticity of the spring) to the positioning repeatability is constant. In this case, the positioning repeatability only depends on the variation force or the coefficient friction that appears between the segment and the slide, consequently the quantification of the tribological error on the positioning repeatability.

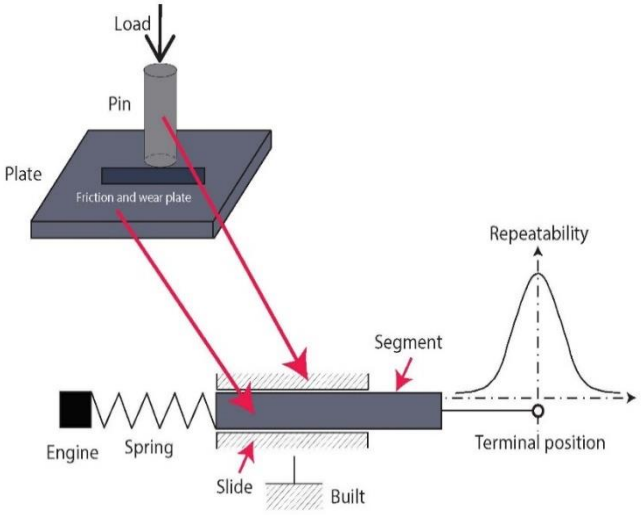

Fig. 3 - Simulated diagram of the proposed robot [13].

3 Material and methods

3.1 Alternative tribometer

The tribological tests were realized on an alternative tribometer (Figure 4 (a)), it was produced and designed in the Laboratory of Mechanical Structures and Materials Engineering (LISMMA), in Paris. This device measures the frictional force between a pin and a plate which are in point or surface contact. It is characterized by almost sinusoidal sliding speeds obtained by a rod-crank system. This tribometer reproduces the contact between a pin and a plate for stress conditions representative of those encountered in an industrial robot situation. Its general characteristics are summarized in Figure (4 (b)).

a) Alternative tribometer used

Type of contact	**Punctual, linear, surface**
Sliding speed	Alternative movement
	Race: from 1 to 50 mm
	Frequency: 0.01 to 10 Hertz
Normal load	20 to 500 N
Atmosphere	Air between 20 - 200 °C
	Immersion in Liquid Nitrogen at -196 °C or in a liquid (between -20 - 100 °C)

b) General characteristics of the tribometer

Fig. 4 - Photo and characteristics of the alternative tribometer.

An arm is used with a double pivot joint, one allowing the application of normal force, and the other in the perpendicular direction, ensuring a degree of freedom for the measurement of friction. The normal force is generated at the end of the arm employing marked masses, and a force sensor measures the frictional force with gauges along the course covered. The TA software and the VCTM2 signal are used to acquire and record the friction forces on a microcomputer.

3.2 Operating conditions

The main tribometer settings, used in this study, are presented in the following table.

Table 1 - Test conditions.

Parameters	Values
Normal force	40 N and 150 N
Sliding speed	80 mm/s
Frequency	1 Hz
Lubrication	Mobilux EP2 grease
Sliding race	40 mm
Duration	1 h
Measure	Friction force

3.3 Materials of the contact couples used

These conditions have chosen to simulate the operating conditions of industrial robots. The test pieces used on the tribometer are a plate representing a steel slide 42CD4 (raw, treated), and a pin representing a segment made of 100C6 steel.

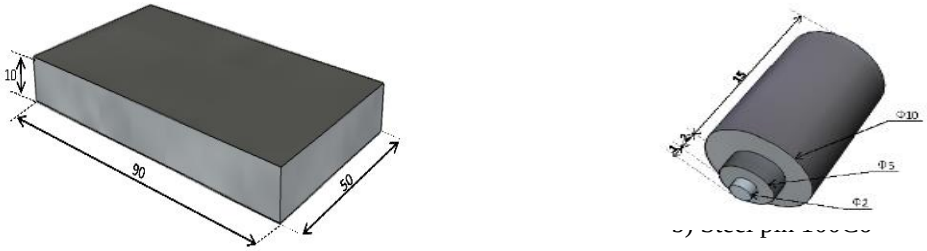

Fig. 5 - Test samples: a) Plate, b) Pin.

4 Results and discussion

4.1 Evolution of the friction coefficient

The Figure. 6 illustrates the friction coefficient variations, which are determined by three tribological tests as a function of the number from cycles with states of the different test pieces morphology (raw, treated) under a normal force 40N and 150N.

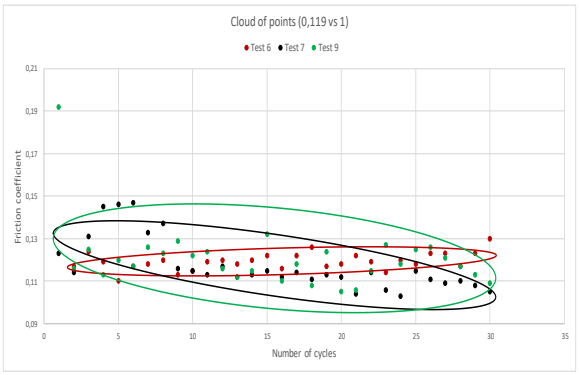

a) 42CD4 raw Fn = 150N

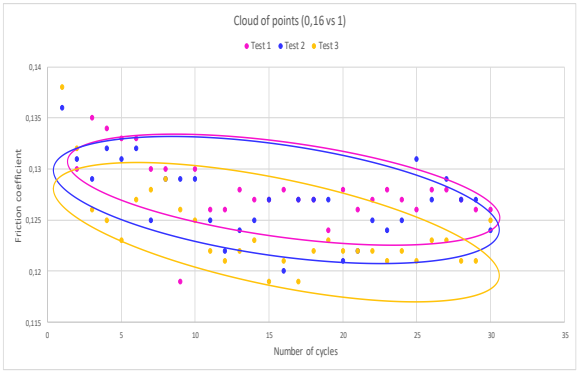

b) 42CD4 treaty Fn = 150N

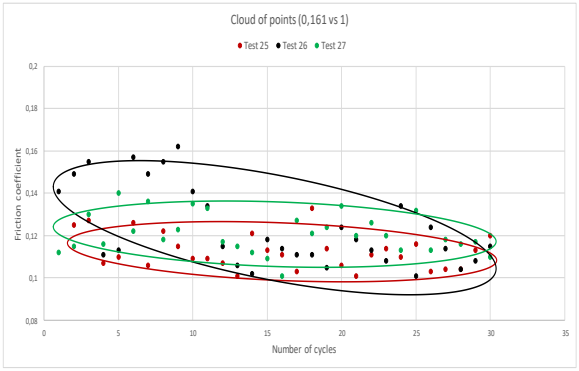

c) 42CD4 raw Fn = 40N

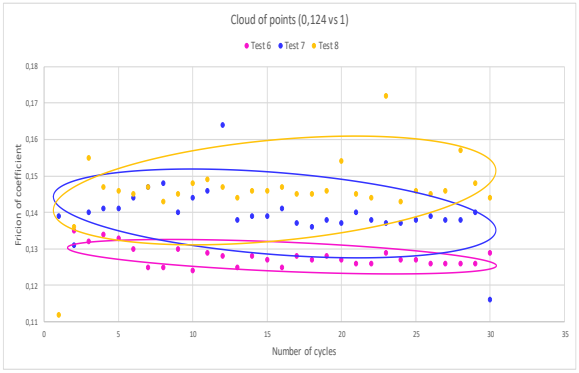

d) 42CD4 treaty Fn = 40N

Fig. 6 - Stochastic modeling of the average friction coefficients of steel 42CD4.

It is observed that the values of the friction coefficient are higher for the raw state than those of the treated state for Fn of 40N. Whereas, for Fn of 150N, the friction coefficient becomes essential for the raw samples but low in the case of the treated samples. This is due to the resistance of the samples to the penetration of the pin. The deeper the penetration, the sliding of the pin becomes difficult, and consequently, the friction coefficient increases. Therefore, for a large normal force (150N), the penetration is essential in the raw samples but less critical in the treated samples because of the surface hardening. Thus, the friction coefficient is controlled by plastic deformation. The average values of the friction coefficient, from one test to another, under the same conditions, are dissipated from the first cycles. It ranges for the two normal forces between 0.09 and 0.16 for raw steel, between 0.115 and 0.16 for treated steel. The results obtained allow us to conclude that the significant variations in the friction coefficient do not depend on the constant sliding speed. Still, it depends on the events which take place at the interface of the antagonist parts, which themselves evolve with the applied load. According to [14] and [15], the friction forces/couples depend not only on the speed but also on the load applied in the case of robots used under a variable load. This behavior can, therefore, appear in a mixed lubrication regime. The friction forces are then a function of the surface state, not of the speed. When the displacement increases progressively, the connection undergoes a rupture at the level of the surfaces in contact, which causes a regime of raw sliding. This detachment movement is related to various characteristics: the texture of the surface, and the contact such as topography, hardness as well as the metallurgy of the surface layers, [16]. This change in friction coefficient values is due to a loss of energy in the form of surface heat dissipated in the two antagonist parts (slide-segment) and to the plastic deformation from which a measurement of the contact surface was random and uncertain. The heat leads to a local temperature increase, which should be evaluated. Thus, the temperature rise within the contact is proportional to the average contact pressure and the friction coefficient. As the thermal coefficients may depend on the speed, the temperature is not precisely proportional to the sliding speed. Thermal dissipation in a localized contact. Hence, the friction coefficient variations are due to distinction criteria between asperities, which are in contact, and those who are not it becomes necessary. For a

low friction coefficient, the asperities do not touch, and therefore the load is supported by the lubricant used, while for large values, the asperity is in contact. Thus, the load is supported in part by the latter. The results obtained allow us to conclude that the friction coefficient values vary around an average value. This inspired us to present a statistical distribution of these values.

4.2 Statistical analysis of results

Our work is based on a statistical analysis of the friction coefficient with probability density function, such as Gaussian or lognormal or uniform laws. Figure. 7 gives the statistical distribution of the friction coefficient, which is generated between the two antagonist pieces. This illustrates the variability of the values. The values analysis of the friction coefficient distribution reveals two principal observations. The first one is a uniform distribution. However, it is conditioned by the duration of the constancy of the friction coefficient for the raw samples. The uniform distribution is due to the sufficient presence of grease, which decreases or eliminates the steel-steel contact. In this case, the grease controls the friction coefficient, which prevents interaction between the surfaces in contact. Secondly, a Gaussian distribution for the treated samples is due to the development of the statistical description of asperity shapes.

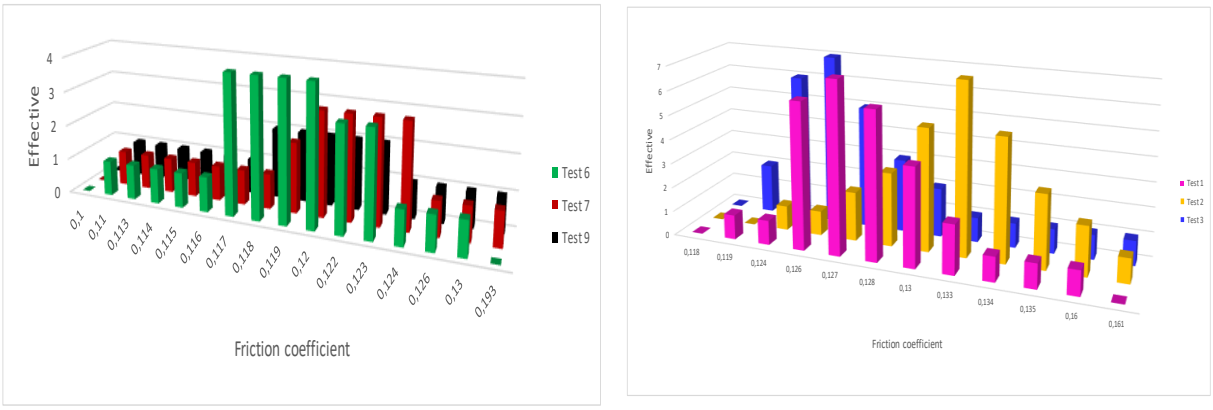

a) 42CD4 raw b) 42CD4 treaty

Fig. 7 - Histograms of the average friction coefficients of steel 42CD4.

The modeling of microgeometry intended to analyze the contact between two surfaces takes into account the shape of the asperities, the geometric characteristics of the asperities, such as the dispersion, the radius, and the deformation can undergo, which can be elastic, elastoplastic and plastics [17]. Another geometrical characteristic plays a primordial role in the contact between two surfaces and distribution from the heights and peaks of the asperities. This observation led us to continue this work from a statistical approach of the contact between Gaussian random surfaces. The model of the random surface and the statistical distribution of the summit and radius are shown in Figure. 8. The variabilities of height and radius give several situations.

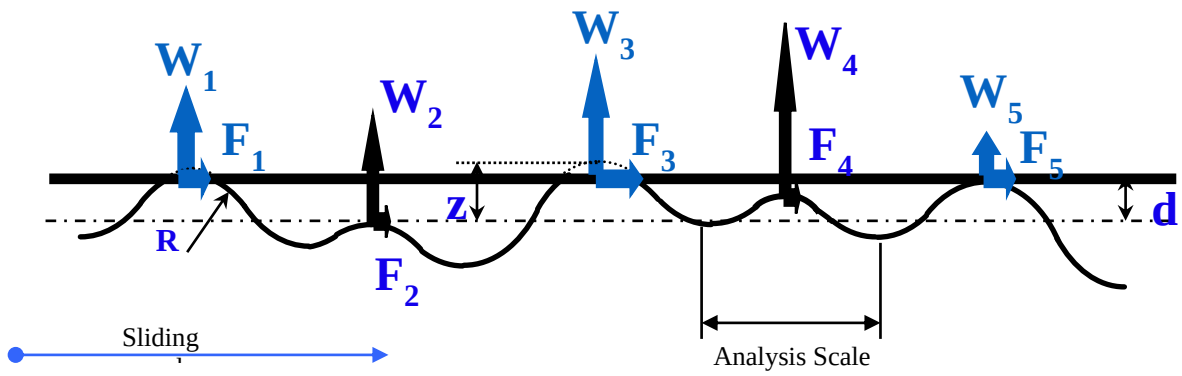

Fig. 8 - Model of contact between surfaces and distribution for the summit altitudes and the radius of asperities.

where R is the radius of asperity; d is a given position counted from the mean line; W_1, W_2, W_3, W_4, W_5 are respectively the normal elasto-plastic, hydro-dynamic, plastic, elasto-hydro-dynamic and elastic forces; and F_1, F_2, F_3, F_4, F_5 are respectively the tangential elasto-plastic, hydro-dynamic, plastic, elasto-hydro-dynamic and elastic forces.

For the first distribution from the altitudes of the asperity peaks, our study considered the proposition for Greenwood and Williamson for the z value of the peak altitude, and it got the following subsequent gaussian law:

$$p_1(z) = \frac{1}{SAlt\sqrt{2\pi}} \exp\left[-\frac{1}{2}\left(\frac{z - Alt}{SAlt}\right)^2\right] \quad (1)$$

where $P_1(z)$ is statistical distribution of peak altitude; z is summit altitude of asperity; and Alt and SAlt are mean and root mean square of the peak altitude.

The second, concerning the radius distribution, this observation was confirmed for random surface [10,12] and proved great caution must be exercised when using merely an estimation of the mean value of the asperity radius. The large variability of radius values justifies the use of a lognormal distribution, which can be given by the formula below instead of a classical normal distribution. This gives negative values for the radius, which is a high probability.

$$p_2(R^*) = \frac{1}{aR^*\sqrt{2\pi}} \exp\left[-\frac{1}{2a^2}\left(\log R^* - b\right)^2\right] \quad (2)$$

where R* is adimensional expression of radius R; R is the radius of asperity; a and b are constants for radius distribution.

In our study, the density function of the probability p (z, R) results from a probability of the altitude of the peak and probability of the radius.

$$p(z,R) = p_1(z) \cdot p_2(R^*) \quad (3)$$

Figure. 9 shows such a surface distribution obtained by the process of grinding. As it reveals, the surface displays high curvature and peak height variations.

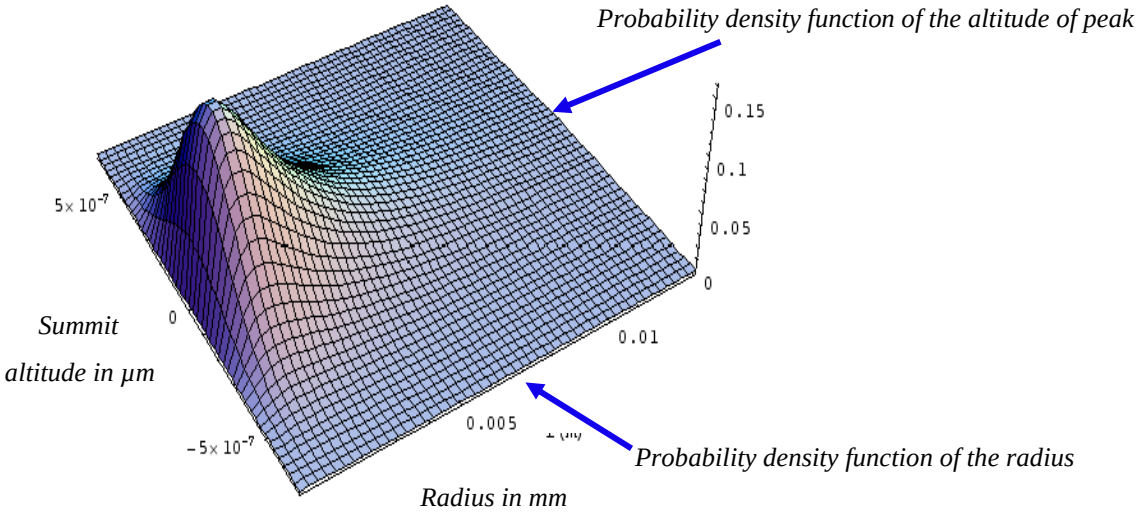

Fig. 9 - Density probability function of asperities as a function of radius and summit altitude p(z,R).

This remark allows us to conclude that the probability density obtained on a profile does not correspond to probability on the surface, because the pattern usually does not occur in general pass precisely at the summit of the peak. Our work, which covers a wider variety of surfaces, also has no way of solving the problem, and for the peaks and summit, it's in the same distribution as ours. The work of Nayak [10] underlines this difference and describes the parameters which can differ in the two approaches on isotropic surfaces. He suggests reserving the term "summit" for a local maximum on a surface and using the notation "peak" for local maxima on a profile. The solution taken by us was to use the D_s and D_1 relationship for random surfaces, which was suggested by him.

$$D_s = 1.2D_1^2, D_1 = \frac{1}{AR} \tag{4}$$

where AR is mean square of the ARi values; ARi is horizontal distance between the peaks of the motif I; and Ds is surface density of asperity.

Therefore obtaining

$$D_s = \frac{1.2}{AR^2} \tag{5}$$

Finally, the probability density can determine the number of asperities, with radius, and the summit altitude between given values. If the contact surface of Aa is apparent, the total number of asperities is, and the number of asperities with a summit between z_1 and z_2 and radius between R_1 and R_2 is

$$\frac{1.2A_a}{AR^2}\int_{z_1}^{z_2}\int_{R_1}^{R_2} p(z,R)dzdR \tag{6}$$

4.3 Characterization of repeatability

The analysis of the positioning errors for the proposed robot's terminal organ is based on a graphic presentation of the point cloud distribution for the desired position. To do this, we used the direct geometric model, and we varied the joint variables (joint friction). Mixed friction results from a partition of the contact into a fraction working in a thick film lubrication situation and the rest working in a thin film. This partition results from a lubricant thickness insufficient to compensate for fluctuations due to the micro-geometry of the surfaces. The following figures show the result obtained.

By analyzing these graphs, we observe that by repetition, the terminal organ always returns to the desired position (exact position) in Figure 10. For this, the robot reaches these desired positions precisely. Only on the displacements of the transmission elements ε_t whose positioning error is assumed to be constant beforehand these positions depend. This observation allows us to conclude that when the friction is zero ($\mu = 0$), the robot's terminal position remains the same. This is justified with the fact that when the energy dissipated at the level of zero contact, the dispersion of the repeatability is also zero. In this case, the shape of the point cloud gathers to a sphere, and this result confirms the result found by the ISO9283 standard because the behavior is isotropic. We consider this graph as a reference.

In Figures 11, 12 and 13 the organ terminal does not always return to the desired position (exact position). In the Figure. 11, we have shown the influence of constant friction ($\mu = 0.12$) on the pose repeatability was revealed. The analysis results showed that the friction coefficient (energy spent) changes the robot's terminal position. The change in position is due to a loss of power in the form of surface heat dissipated in the two-antagonist slide-segment pieces, resulting in a dispersion of repeatability that is constant and non-zero. The

results obtained allow us to conclude that the dispersion of repeatability ε_D depends on the displacement of the transmission elements ε_t supposed constant but increased by ε_{D2} and reduced by ε_{D1} (adjusted in excess or by default) with the dispersion of friction. In this case, the dispersion describes a point cloud on either side of the reference circle. Regarding Figure 12, we evaluated the field of repeatability for a Gaussian variation of the friction coefficient. This latter depends on the events that take place at the interface of the antagonist's part. The variability of the values from the friction coefficients is already analyzed previously. In this case, the dispersion of repeatability ε_D will depend on the displacement of the transmission elements ε_t with a variation of the limits of the distribution. However, the dispersion of repeatability due to friction will widen the preceding dispersion band between a zero effect ε_{D1} and a maximum effect ε_{D2}, which will correspond to the average friction coefficient. Finally, the Figure. 13 shows the uniform variation of the friction coefficient. This distribution is similar to constant friction (μ = 0.12). However, it is conditioned by the constancy duration of the friction coefficient. The dispersion cloud is additional to the dispersion circle due to the displacements of the transmission elements ε_t, where the band widens and narrows from the dispersion circle according to the value of the friction coefficient.

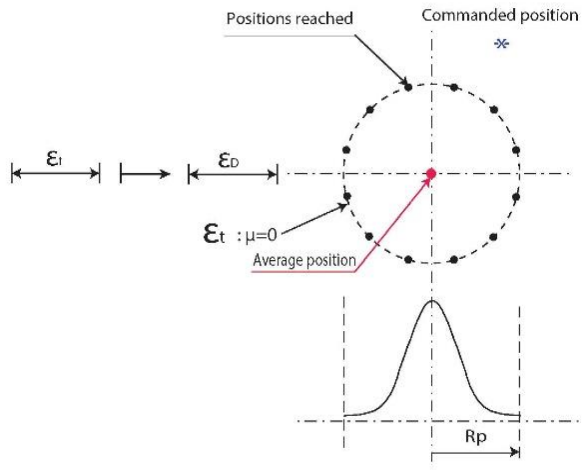

Fig. 10- Represents ε_D-ε_t for zero friction.

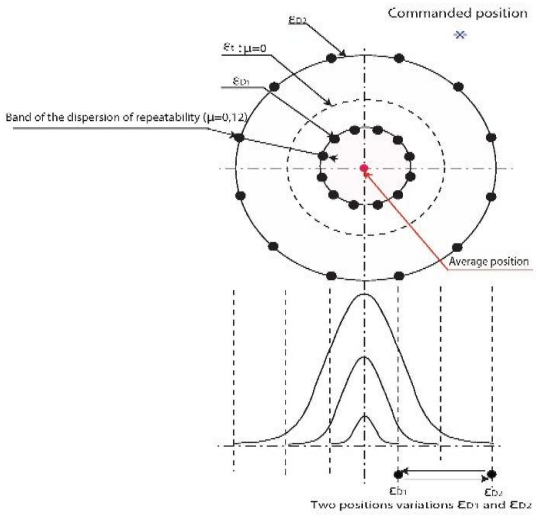

Fig. 11 - Repeatability field in µm for constant friction.

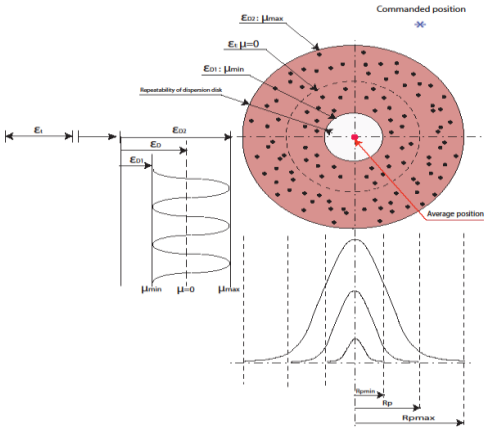

Fig. 12 - Repeatability field in µm for a Gaussian variation of friction coefficient.

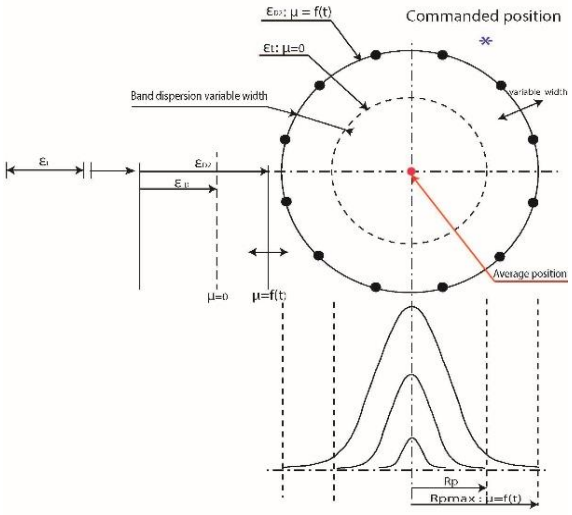

Fig. 13 - Repeatability field in µm for a uniform variation of friction coefficient.

where Rp is the pose repeatability ; R_{pmax} is the maximum pose repeatability ; R_{pmin} is the minimum pose repeatability ; ε_D is the dispersion of repeatability ; ε_t is the displacement of transmission elements ; ε_{D1} is the

minor dispersion of repeatability ; ε_{D2} is the major dispersion of repeatability ; μ is the friction coefficient ; μ_{max} is the maximum friction coefficient ; and μ_{min} is the minimum friction coefficient.

5 Conclusion

The positioning repeatability was investigated through the industrial robot's output element as a function of the tribological behavior for the segment-slide couple simulated by the pin-plate couple from the alternative tribometer. The evolution of the friction coefficient of these latter was followed. Due to the variability of the friction coefficient values, it is necessary to analyze the dimension variability of the asperities in the case of non-periodic microgeometry. This analysis allowed us to select three parameters, particularly the distance between two consecutive asperities, the radius along an asperity and its altitude. It is shown that repeatability responds favorably to the statistical model represented by a sphere and that the repetitive positioning of the terminal organ of the robot follows a statistical distribution with probability density functions such as Gaussian or lognormal laws, which allow us to derive a complete distribution around the commanded position. This modeling makes it possible to better characterize the robot's repeatability, and to understand the tribological behavior of surfaces in contact. This will help us to include them into numerical procedures or program subroutines, and then use them in particular tiny assembling operations or in micromanipulation.

REFERENCES

[1] ISO, "ISO 9283:1998", ISO. https://www.iso.org/cms/render/live/en/sites/isoorg/contents/data/standard/02/22/22244.html (accessed Jun. 11, 2020).

[2] E. Ramsli, "Probability Distribution of Repeatability of Industrial Robots", Int. J. Robot. Res., vol. 10, no. 3, pp. 276-283, Jun. 1991, doi: 10.1177/027836499101000308.

[3] Y. Edan, L. Friedman, A. Mehrez, and L. Slutski, "A three-dimensional statistical framework for performance measurement of robotic systems", Robot. Comput.-Integr. Manuf., vol. 14, no. 4, pp. 307-315, Aug. 1998, doi: 10.1016/S0736-5845(98)00006-4.

[4] R. Riemer and Y. Edan, "Evaluation of influence of target location on robot repeatability", Robotica, vol. 18, pp. 443-449, Jul. 2000, doi: 10.1017/S0263574799002337.

[5] O. Felix Offodile and K. Ugwu, "Evaluating the effect of speed and payload on robot repeatability", Robot. Comput.-Integr. Manuf., vol. 8, no. 1, pp. 27-33, Jan. 1991, doi: 10.1016/0736-5845(91)90004-C.

[6] A. Hijazi, "Contribution to the Analysis and Exploitation the Singularities to Improve the Precision of Mechatronic Systems", Normandie Université, 2017.

[7] J.-F. Brethé, E. Vasselin, D. Lefebvre, and B. Dakyo, "Modelling of repeatability phenomena using the stochastic ellipsoid approach", Robotica, vol. 24, no. 4, pp. 477-490, Jul. 2006, doi: 10.1017/S0263574705002481.

[8] B. Bona and M. Indri, "Friction Compensation in Robotics: an Overview", in Proceedings of the 44th IEEE Conference on Decision and Control, Dec. 2005, pp. 4360-4367, doi: 10.1109/CDC.2005.1582848.

[9] J. A. Greenwood, J. B. P. Williamson, and F. P. Bowden, "Contact of nominally flat surfaces", Proc. R. Soc. Lond. Ser. Math. Phys. Sci., vol. 295, no. 1442, pp. 300-319, Dec. 1966, doi: 10.1098/rspa.1966.0242.

[10] P. R. Nayak, "Random Process Model of Rough Surfaces", J. Lubr. Technol., vol. 93, no. 3, pp. 398-407, Jul. 1971, doi: 10.1115/1.3451608.

[11] P. R. Nayak, "Some aspects of surface roughness measurement", Wear, vol. 26, no. 2, pp. 165-174, Nov. 1973, doi: 10.1016/0043-1648(73)90132-4.

[12] D. J. Whitehouse, J. F. Archard, and D. Tabor, "The properties of random surfaces of significance in their contact", Proc. R. Soc. Lond. Math. Phys. Sci., vol. 316, no. 1524, pp. 97-121, Mar. 1970, doi: 10.1098/rspa.1970.0068.

[13] A. Rezala and M. Arbaoui, "Analysis Randon Causes Repeatability Errors Inducted by Friction at Joints in Industrial Robots ", IJE TRANSACTIONS B: Applications, Vol. 35, No. 02, (February 2022), pp.

451-457, doi: 10.5829/ije.2022.35.02b.21.
[14] G. Abba and P. Sardain, "Modélisation des frottements dans les éléments de transmission d'un axe de robot en vue de son identification", Mécanique Ind., vol. 4, no. 4, pp. 391-396, Jul. 2003, doi: 10.1016/S1296-2139(03)00074-5.
[15] P. Hamon, M. Gautier, and P. Garrec, "Dynamic identification of robots with a dry friction model depending on load and velocity", in 2010 IEEE/RSJ International Conference on Intelligent Robots and Systems, Oct. 2010, pp. 6187-6193, doi: 10.1109/IROS.2010.5649189.
[16] B. Armstrong-Hélouvry, P. E. Dupont, and C. C. de Wit, "A survey of models, analysis tools and compensation methods for the control of machines with friction", Autom., 1994, doi: 10.1016/0005-1098(94)90209-7.
[17] J. Huang, C. Gao, C. Zhou, and X. Lin, "Effect of solid body contact deformation on the real contact area under the thermo-mechanical coupling", Aust. J. Mech. Eng., vol. 14, no. 1, pp. 44-52, Jan. 2016, doi: 10.1080/14484846.2015.1093207.